Applied Catalysis B: Environmental 245 (2019) 314–324

Contents lists available at ScienceDirect

Applied Catalysis B: Environmental

journal homepage: www.elsevier.com/locate/apcatb

CO oxidation over supported Pt/$Cr_xFe_{2-x}O_3$ catalysts and their good tolerance to CO_2 and H_2O

Ting Wang, Jin-Yuan Xing, Li Zhu, Ai-Ping Jia, Yue-Juan Wang, Ji-Qing Lu*, Meng-Fei Luo*

Key Laboratory of the Ministry of Education for Advanced Catalysis Materials, Institute of Physical Chemistry, Zhejiang Normal University, Jinhua 321004, China

ARTICLE INFO

Keywords:
CO oxidation
Pt catalyst
$Cr_{1.3}Fe_{0.7}O_3$ solid solution
Corundum structure
CO_2 and H_2O tolerant

ABSTRACT

Pt catalysts supported on a series of $Cr_xFe_{2-x}O_3$ composite oxides with different Cr/Fe molar ratios were prepared and tested for CO oxidation. The Pt/$Cr_{1.3}Fe_{0.7}O_3$ catalyst possesses the best performance (with a turnover frequency of ca. 0.2 s^{-1} at 80 °C under 1% CO + 1% O_2 condition), due to its best reducibility which was related to the solid solution structure of the support. The catalyst also shows good stability in the presence of both 10% CO_2 and 10% H_2O. Detailed kinetic results and staged reaction indicate that CO_2 and H_2O play opposite roles in the reaction. The inhibiting role of CO_2 is due to competitive adsorption of CO_2 with CO and the formation of carbonate species. However, the addition of H_2O could effectively decompose the carbonate and sustain the catalyst stability. Moreover, the promoting role of H_2O could be mainly attributed to the weakened strength of CO adsorption and the fast interfacial reaction between CO and the surface hydroxyl groups formed via H_2O dissociation, as revealed by the X-ray photoelectron spectroscopy, CO temperature-programmed desorption and the kinetic results.

1. Introduction

Catalytic CO oxidation over various catalyst systems such as Au [1–5] and Pt [6–10] has been extensively investigated as an ideal model reaction to probe the structure - performance relation and the nature of active sites [11]. This reaction has also been practically applied in automotive exhaust abatement [12] and proton exchange membrane fuel cell (PEMFC) [13]. In general, CO oxidation in model reaction is usually conducted under dry condition (CO + O_2), while the reactants in practical conditions contain large amount of CO_2 and H_2O (i.e. higher than 10 vol.%) in addition to CO and O_2 [14]. Consequently, the presence of CO_2 and/or H_2O exerts remarkable influences in the behaviors of the catalysts, and in most cases dramatic catalyst deactivation is observed [15–18], particularly in the presence of both CO_2 and H_2O. The inhibiting role of CO_2 has been unequivocally attributed to the blockage of active sites by the competitive adsorption of CO and CO_2 and the formation of surface carbonate species [19]. However, the role of H_2O is debatable. Landen et al. [20] reported that the addition of 4 wt.% H_2O in the feed stream drastically suppressed the CO conversion from 40% to less than 5% on a Au/Fe_2O_3 catalyst at 25 °C. Similar deactivation was also observed on the Pt/CeO_2 catalyst, as the addition of 5 vol. % H_2O in the feed decreased the CO conversion [15]. In contrast, more works on either Au [21,22] or Pt [23,24] catalysts reveal obvious promoting effect of H_2O, which is believed to be due to the decomposition of surface carbonate species by moisture and/or the involvement of H_2O/hydroxyl groups in CO oxidation [25]. However, it must be noted that such promoting effect of H_2O could be achieved only at low H_2O concentrations, while at high concentrations, the presence of H_2O could inhibit the activity. For example, Ojeda et al. [26] found that the CO oxidation activity over a Au/Al_2O_3 catalyst continuously increased in H_2O concentrations from 0.03 - 0.5 vol. %; however, the activity declined at high H_2O concentrations (> 0.5 vol. %), which was attributed to the competitive adsorption of H_2O and CO.

For the purpose of practical application, the catalyst stability under realistic conditions is extremely important. Unfortunately, the commonly observed catalyst deactivation as above-mentioned makes this target very challenging. Iron oxide (FeO_x) is a promising support or promoter for noble metals (such as Au, Pt and Ir) for CO oxidation due to its ability to supplying or generating active oxygen species [27–29] However, such FeO_x-containing catalysts usually deactivate rapidly in the presence of large amount of CO_2 and/or H_2O [20]. One possible approach to overcome this disadvantage is to modify the FeO_x support because it could significantly alter the catalyst properties and consequently catalytic behaviors [18]. On the other hand, chromium oxide (CrO_x) has also been used as an effective component in CO oxidation. For example, Xanthopoulou and Vekinis [30] reported that the Cu-Cr-O spinel oxide is an promising support for Pd, which gives much higher activity than the Pd/Al_2O_3 in CO oxidation. Moreover, the spinel oxide

* Corresponding authors.
E-mail addresses: jiqinglu@zjnu.cn (J.-Q. Lu), mengfeiluo@zjnu.cn (M.-F. Luo).

https://doi.org/10.1016/j.apcatb.2018.12.054
Received 9 August 2018; Received in revised form 26 November 2018; Accepted 22 December 2018
Available online 27 December 2018
0926-3373/

itself (support alone without Pd) has comparable activity as the Pd/Al_2O_3 catalyst in CO oxidation due to the synergy between Cr and Cu species. Pantaleo et al. [31] also reported that the formation of Cu-Cr-O mixed oxides are beneficial for the improvement of CO oxidation activity. Particularly, the Cr-based mixed oxides show some good resistance to H_2O, as our previous work [32] demonstrated the highly active $CoCr_2O_4$ spinel oxides are stable for CH_2Cl_2 combustion in the presence of 12,000 ppm water vapor. These findings in literature inspire us that a combination of Cr and Fe might show some potential in the synthesis of active and stable catalysts for CO oxidation under realistic conditions. Therefore, in this work, we synthesized a series of $Cr_xFe_{2-x}O_3$ composite oxides as the supports for Pt catalysts, and the main target of the current work is to investigate whether these catalysts are stable in the presence of CO_2 and H_2O in the CO oxidation environment. Indeed, it is found that some catalysts with specific Cr/Fe molar ratios show very good performance under dry condition (CO + O_2), which is better than that supported on bare CrO_x or FeO_x. The most interesting finding is that some catalysts are highly tolerant to the high concentrations of CO_2 and H_2O, which makes them potential in practical applications. Moreover, detailed kinetic investigation is carried out to explain the behaviors of the catalysts under different reaction conditions (i.e. CO + O_2, CO + O_2 + CO_2, CO + O_2 + H_2O and CO + O_2 + CO_2 + H_2O). Based on the experimental results, the roles of CO_2 and H_2O are discussed.

2. Experimental

2.1. Catalyst preparation

The $Cr_xFe_{2-x}O_3$ composite oxides with different Cr/Fe molar ratios (4/1, 2/1, 1/1 and 1/4) were prepared using a sol-gel method. Cr$(NO_3)_3{\cdot}9H_2O$ (99.8%), Fe$(NO_3)_3{\cdot}9H_2O$ (99.5%) and citric acid (99.0%) with a citric acid / (Cr + Fe) molar ratio of 2 were dissolved in deionized water, which was then slowly heated at 90 °C until a viscous gel was formed. The dry gels were dried at 120 °C for 12 h and calcination at 500 °C for 4 h to obtain the supports, which were denoted as $Cr_xFe_{2-x}O_3$. The pure Cr_2O_3 and Fe_2O_3 oxides were prepared with a similar manner, using Cr$(NO_3)_3{\cdot}3H_2O$ and Fe$(NO_3)_3{\cdot}9H_2O$ as the precursors, respectively.

The Pt catalysts supported on the oxides were prepared by an incipient wetness impregnation and the nominal Pt content was 2 wt.%. For example, 4.9 g of the support was immersed by 20 ml of Pt$(NO_3)_2$ aqueous solution with a Pt content of 0.005 g ml^{-1}. After the mixture was kept at r.t. for 3 h, it was evaporated at 90 °C in a water bath and dried at 100 °C for 4 h and calcined at 300 °C for 4 h to obtain the final catalyst. The catalysts were denoted as Pt/$Cr_xFe_{2-x}O_3$. For comparison, a Pt supported on a mechanically mixed Cr_2O_3 and Fe_2O_3 with a nominal Cr/Fe molar ratio of ca. 2 was also prepared in a similar manner for comparison, and it was denoted as Pt/1.3CrO_x-0.7FeO_x.

2.2. Catalyst characterizations

The actual contents of the metal elements in the catalysts were determined by inductively coupled plasma-atomic emission spectrometry (ICP-AES) on an IRIS Intrepid 2 instrument. The specific surface areas of the supports and catalysts were measured by N_2 adsorption at 77 K on a surface area analyzer (Quantachrome Autosorb-1). X-ray powder diffraction (XRD) patterns of the catalysts were recorded on a powder X-ray diffractometer (Bruker D8 ADVANCE), operated at 40 kV and 40 mA, using Cu K_α radiation. The average crystallite sizes and the lattice parameters of the samples were analyzed by the Topas software.

High-resolution transmission electron microscopy images of the catalysts were obtained on a JEM-2100 F microscopy operated at 200 kV. The samples were reduced at 200 °C for 1 h in 5% H_2-95% Ar (30 ml min^{-1}). Hydrogen temperature - programmed reduction (H_2-TPR) experiments were carried out in a home-made apparatus. Ten mg of the catalyst was loaded in a quartz reactor and was heated from r.t. to 800 °C (10 °C min^{-1}) in a 5% H_2 - 95% N_2 gas (30 ml min^{-1}). The H_2 consumption signal was recorded by a thermal conductivity detector (TCD), which was quantified by the reduction of CuO powder with a known amount.

X-ray photoelectron spectra (XPS) of the catalysts were measured on an ESCALAB 250Xi instrument, using an Al Kα X-ray source (1486.6 eV). The binding energies (BEs) of the surface species were calibrated using C1 s core level at BE of 284.8 eV. For the measurement of the pre-reduced catalyst, the catalyst was reduced with an 5%H_2 - 95% N_2 mixture (30 ml min^{-1}) at 200 °C for 1 h in a pretreatment chamber. After cooling down, it was transferred to the analysis. For the treatment of CO_2, after the pre-reduced sample (5% H_2 - 95% N_2 mixture (30 ml min^{-1}) at 200 °C for 1 h) was cooled down to 80 °C, it was exposed to a flow of 10% CO_2 + 90% N_2 for 1 h and then transferred to the analysis chamber. After the analysis, the sample was again moved to the pretreatment chamber and exposed to 10% H_2O vapor + 90% N_2 at 80 °C for 1 h and transferred to the analysis chamber. Note that the above-mentioned procedures were performed inside the instrument without being exposed to air.

CO temperature-programmed desorption (CO-TPD) experiments were carried out on a quartz reactor. Fifty mg of the catalyst was pretreated with 10% O_2 - 90% He (30 ml min^{-1}) and subsequent pure He (30 ml min^{-1}) at 300 °C for 1 h, then it was cooled down to 30 °C and purged for 30 min in a He flow (30 ml min^{-1}). A flow of 1% CO + 99% Ar (30 ml min^{-1}) or 1% CO + 10% CO_2 + 89% Ar (30 ml min^{-1}), or 1% CO + 10% H_2O vapor - 89% Ar (30 ml min^{-1}) was then introduced for 30 min. The catalyst was purged by a He flow (30 ml min^{-1}) for 30 min to remove the gas phase or weakly adsorbed molecules, and was heated from 30 to 400 °C at a ramp of 10 °C min^{-1} in the He flow. The desorption signals of CO and CO_2 were recorded by a mass spectrometer (MS, HIDEN QIC-20) at m/e = 28 and 44, respectively. To investigate the CO desorption behaviors under the real condition (as the catalyst was pre-reduced before reaction), the sample was also pretreated with 10% O_2 - 90% He (30 ml min^{-1}) and subsequent 10% H_2 - 90% He (30 ml min^{-1}) at 200 °C for 1 h, then it was cooled down to 30 °C and purged for 30 min in a He flow (30 ml min^{-1}). And the above described procedure was performed. O_2 temperature -programmed desorption (O_2-TPD) experiments were carried out on the same equipment as in the CO-TPD. One hundred mg of the sample was loaded and pretreated with 10% O_2 + 90% Ar (30 ml min^{-1}) at 300 °C for 1 h and cooled down to 30 °C. The sample was then purged with Ar (30 ml min^{-1}) until the MS signal is stabilized, and was heated from 30 to 600 °C with a ramp of 10 °C min^{-1}, and the desorption signal of O_2 was recorded at m/e = 32. The sample was also pretreated with 10% O_2 + 90% Ar (30 ml min^{-1}) at 300 °C for 1 h followed by 10% H_2 + 90% Ar (30 ml min^{-1}) at 200 °C for 1 h, and the above described procedure was performed.

2.3. CO oxidation and kinetic investigation

The reaction was conducted in a tubular quartz reactor (i.d. = 6 mm) at atmospheric pressure. Fifty mg of the catalyst (particle size = 0.12 - 0.15 mm) diluted with 100 mg of quartz sand with same size was loaded in the reactor. Before reaction, the catalyst was pre-reduced with a flow of 5%H_2 - 95% Ar (15 ml min^{-1}) at 200 °C for 1 h. After it was cooled down to certain temperature and a gas mixture consisting of 1% CO + 1% O_2 + 98% N_2, or 1% CO + 1% O_2 + 10% CO_2 + 88% N_2, or 1% CO + 1% O_2 + 10% H_2O + 88% N_2, or 1% CO + 1% O_2 + 10% CO_2 + 10% H_2O + 88% N_2 was introduced with a total flow rate of 100 ml min^{-1} (space velocity (S.V.) = 120,000 ml g_{cat}^{-1} h^{-1}). The 10% H_2O vapor was introduced by passing the reactants through a saturated H_2O vapor generator at 50 °C. Besides, possible condensation of H_2O vapor in the line was avoided by keeping the inlet line at 60 °C. The CO concentration in the reactants was analyzed by a GC (Agilent 6850) equipped with a TCD detector.

The reaction kinetics were conducted on the same reactor as in the

Table 1
Physical properties of various catalysts.

Catalyst	Pt content / wt.%	Cr/Fe molar ratio	S_{BET} / m^2 g^{-1}	Bulk phase [a]	Crystal. size [a] / nm	Pt size [b] / nm	Pt dispersion [c]	TOF [d] / x 10^{-3} s^{-1}
Pt/Cr_2O_3	1.92	–	31.5	Cr_2O_3	25.4	1.9 ± 0.4	0.58	22.3
$Pt/Cr_{1.6}Fe_{0.4}O_3$	2.34	3.98	17.2	Cr_2O_3	42.6	2.1 ± 0.8	0.52	31.2
$Pt/Cr_{1.3}Fe_{0.7}O_3$	2.05	2.04	14.6	$Cr_{1.3}Fe_{0.7}O_3$	55.3	2.0 ± 0.9	0.55	202.5
$Pt/Cr_{1.0}Fe_{1.0}O_3$	2.18	1.15	52.1	γ-Fe_2O_3	14.0	1.7 ± 0.4	0.65	141.8
$Pt/Cr_{0.4}Fe_{1.6}O_3$	2.51	0.24	46.4	γ-Fe_2O_3	17.5	2.0 ± 0.7	0.55	138.0
Pt/Fe_2O_3	1.94	–	18.2	α-Fe_2O_3	41.8	2.6 ± 0.6	0.42	99.7
$Pt/1.3CrO_x$-$0.7FeO_x$	2.17	2.11	28.1	–	–	–	–	–

[a]: Determined by XRD; [b]: Determined by HRTEM; [c]: Dispersion = $1.1/d_{Pt}$ (d_{Pt} = Pt particle size in nm); [d]: TOF calculated based on Pt dispersion and reaction rate at 80 °C.

catalytic testing. The partial pressures of the feed gases (0.30–3.04 kPa for CO and O_2, 1.01–15.15 kPa for CO_2 and 3.03–15.15 kPa for H_2O) were adjusted by mass flow controllers and balanced by N_2 to keep the total flow rate constant (100 ml min^{-1}). Low CO conversions (less than 15%) and the absence of mass and heat transfer limitations ensured the reaction was in kinetic region (See Supporting Information for detailed calculations).

3. Results and discussion

3.1. Characterization results

Table 1 shows that the actual Pt contents in the supported catalysts are very close to the nominal values (2 wt.%). Also the Cr/Fe ratios in the catalysts are close to their corresponding nominal values. The catalysts have surface areas of 14.6 - 52.1 m^2 g^{-1}, depending on their compositions.

The XRD patterns of the supported catalysts (Fig. 1) show no diffractions related to Pt species, suggesting that those species are highly dispersed on the supports. The patterns of the Pt/Cr_2O_3 and $Pt/Cr_{1.6}Fe_{0.4}O_3$ catalysts give diffractions at 2θ of 24.5, 33.6, 36.2, 41.5, 50.3, 54.8, 58.3, 63.3 and 64.9° assigning to eskolaite with corundum structure (Cr_2O_3, JCPDS No. 38-1479), although the intensities of the peaks are different for the two samples. The pattern of the $Pt/Cr_{1.3}Fe_{0.7}O_3$ is similar to those of the Pt/Cr_2O_3 and $Pt/Cr_{1.6}Fe_{0.4}O_3$, but the diffractions systematically shift to lower angle by 0.1 - 0.2°. The pattern fits well with the structure of chromium iron oxide ($Cr_{1.3}Fe_{0.7}O_3$, JCPDS No. 35-1112), which is a solid solution compound

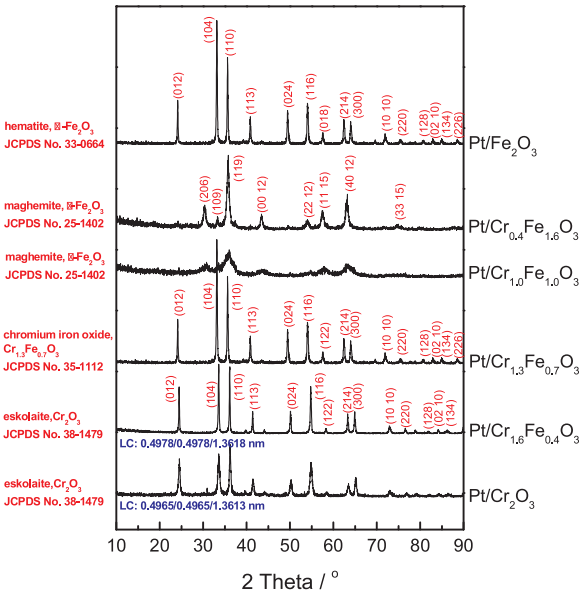

Fig. 1. XRD patterns of various supported Pt catalysts.

with Fe atoms substitute in the Cr_2O_3 matrix (see Fig. S1 for the structural details). The lattice parameters of the $Pt/Cr_{1.6}Fe_{0.4}O_3$ are 0.4978/0.4978/1.3618 nm, which is larger than those of the Pt/Cr_2O_3 (0.4965/0.4965/1.3613 nm) because the ionic radius of Fe^{3+} (0.0645 nm) is larger than that of the Cr^{3+} (0.0615 nm). However, with increasing Fe content in the support, the XRD patterns of the $Pt/Cr_{1.0}Fe_{1.0}O_3$ and $Pt/Cr_{0.4}Fe_{1.6}O_3$ are different from those with low Fe contents. The diffractions at 2θ of 30.4, 33.4, 35.8, 43.6, 54.2, 57.6 and 63.3° are assigned to maghemite (γ-Fe_2O_3, JCPDS No. 25-1402). In contrast, the Pt/Fe_2O_3 gives diffractions at 2θ of 24.2, 33.2, 35.6, 40.9, 49.5, 54.1, 57.6 and 62.5°, which are assigned to hematite (α-Fe_2O_3, JCPDS No. 33-0664). The XRD results clearly indicate that the structural properties vary due to different Cr/Fe molar ratios. Since there is no detection of the mixture of Cr_2O_3 and Fe_2O_3 oxides in these samples, the samples (except for the bare Cr_2O_3 and Fe_2O_3) are in forms of solid-solution-like structure. It is worth noting that the crystal phase changes from Cr_2O_3-based oxide to Fe_2O_3-based oxide when the Cr/Fe molar ratio is less than 1/1. Particularly, the $Pt/Cr_{1.0}Fe_{1.0}O_3$ and $Pt/Cr_{0.4}Fe_{1.6}O_3$ catalysts have a crystal phase of γ-Fe_2O_3 while the Pt/Fe_2O_3 has a crystal phase of α-Fe_2O_3. It is reported that the γ-Fe_2O_3 phase could transform to α-Fe_2O_3 when the oxide is thermally treated at 400–500 °C in air [33]. Therefore, it seems that the cooperation of Cr ions in the Fe_2O_3 matrix could somehow stabilize the γ-Fe_2O_3 phase under high temperature calcination. Also, the crystallite size analyses (Table 1) revealed that the $Pt/Cr_{1.0}Fe_{1.0}O_3$ has the smallest size (14.0 nm) while the $Pt/Cr_{1.3}Fe_{0.7}O_3$ has the largest (55.3 nm).

The HRTEM images of the pre-reduced catalysts (Fig. 2) show that the Pt particles in all catalysts are rather small (1.7–2.6 nm, Table 1). The observation of small Pt particles are in good agreement with the XRD results (Fig. 1), as there is no diffraction of Pt species could be observed. In turn, the Pt dispersions in the catalysts are calculated to be 0.42 - 0.65 (Table 1).

The H_2-TPR profiles of the supports (Fig. 3a) show that the Cr_2O_3 gives overlapped reduction peaks at 200–300 °C due to the reduction of CrO_3 to Cr_2O_3 [34], while the addition of Fe in the support brings an additional reduction peak centered at ca. 380 °C due to the reduction of Fe_2O_3 to Fe_3O_4 [35]. The overlapped reduction of the $Cr_xFe_{2-x}O_3$ samples in 200–400 °C region suggests the simultaneous reduction of CrO_x and FeO_x oxides. Moreover, the profile of the $Cr_{1.3}Fe_{0.7}O_3$ is very different from that of the mechanically mixed $1.3CrO_3$-$0.7FeO_x$, which clearly implies the very differences in the structural properties of these two sample. The Fe_2O_3 support gives peaks centered at 391 and 629 °C, and the latter is assigned to the reduction of Fe_3O_4 to FeO/Fe [36]. The H_2 consumption of the low temperature (LT, temperature below 400 °C) reduction peaks are calculated, and the $Cr_{1.3}Fe_{0.7}O_3$ support shows the highest H_2 consumption (1.45 mmol g^{-1}). In contrast, the mechanically mixed $1.3CrO_x$-$0.7FeO_x$ gives much lower H_2 consumption (0.39 mmol g^{-1}). Such different reducibility of the supports is related to their structural properties and it seems that the $Cr_{1.3}Fe_{0.7}O_3$ solid solution has the best reducibility. In contrast, the supported Pt catalysts show completely different profiles (Fig. 3b). The reduction temperature of the Pt catalysts systematically shift to lower temperatures due to the typical

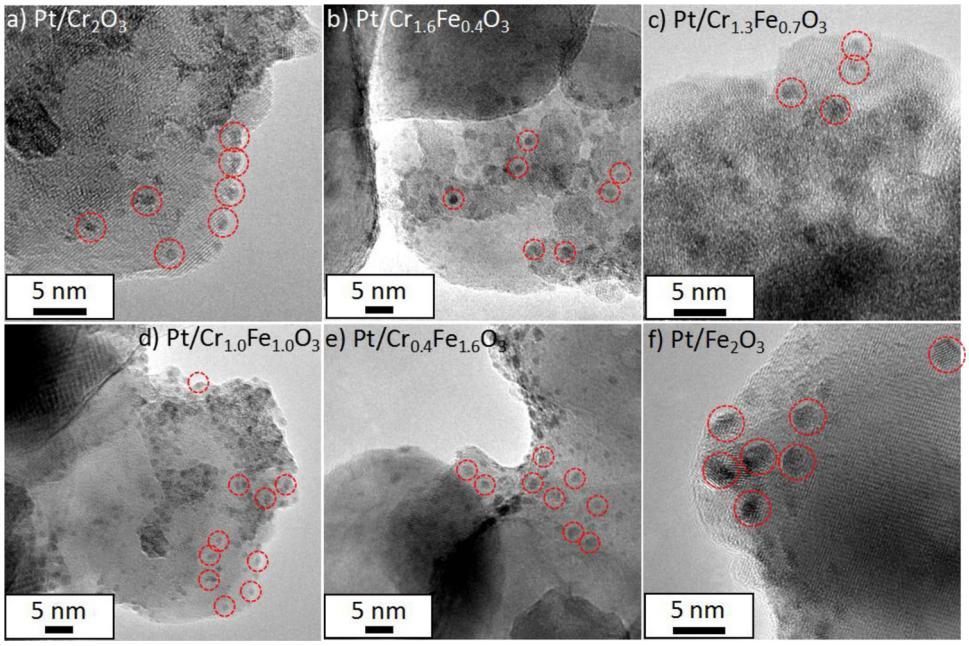

Fig. 2. HRTEM images of pre-reduced various Pt catalysts. Pt species are indicated by red circles. (For interpretation of the references to colour in this figure legend, the reader is referred to the web version of this article).

spillover effect. Particularly, the $Pt/Cr_{1.6}Fe_{0.4}O_3$, $Pt/Cr_{1.3}Fe_{0.7}O_3$, $Pt/Cr_{1.0}Fe_{1.0}O_3$ and $Pt/Cr_{0.4}Fe_{1.6}O_3$ catalysts give sharp reduction peaks below 100 °C, suggesting greatly enhanced catalyst reducibility. Besides, the LT H_2 consumptions of the Pt catalysts are slightly higher than those of the corresponding supports, due to the reduction of Pt oxide. Note that the LT reduction peaks of the Pt catalysts also contain the reduction of support oxides because the maximal nominal H_2 consumption of Pt oxide in the catalysts are 0.2 mmol g^{-1} (assuming the average Pt content in the catalyst is 2 wt.% and all the Pt species are PtO_2), which is much lower than the obtained values.

The oxidation states of the Pt species in some representative catalysts (Pt/Cr_2O_3, $Pt/Cr_{1.3}Fe_{0.7}O_3$ and Pt/Fe_2O_3) were analyzed by XPS and the results are shown in Fig. S2. The Pt $4f_{5/2}$ spectra of the catalysts give two resolved components at BEs of 72.6 and 74.9 eV assigning to Pt^{2+} and Pt^{4+}, respectively [37,38] Also it seems that the Pt^{4+} species are dominant as its peak area is much larger than that of the Pt^{2+}. The analyses of other elements (Fig. S3) reveal that the Cr species are mainly Cr^{3+} (with a small portion of Cr^{6+}), the Fe species are mainly Fe^{3+} and O species are in forms of adsorbed surface oxygen and lattice oxygen. After pre-reduction, the Pt $4f_{5/2}$ spectrum of the $Pt/Cr_{1.3}Fe_{0.7}O_3$ (Fig. S2) gives a component at BE of 71.2 eV assigning to Pt° accompanied by the decline in the intensity of Pt^{4+} species, indicating that some Pt^{4+} species were reduced during the pre-reduction.

3.2. CO oxidation under different conditions

Fig. 4 illustrates the performance of the catalysts at reaction temperature of 80 °C under various reaction conditions. 1. Under 1%

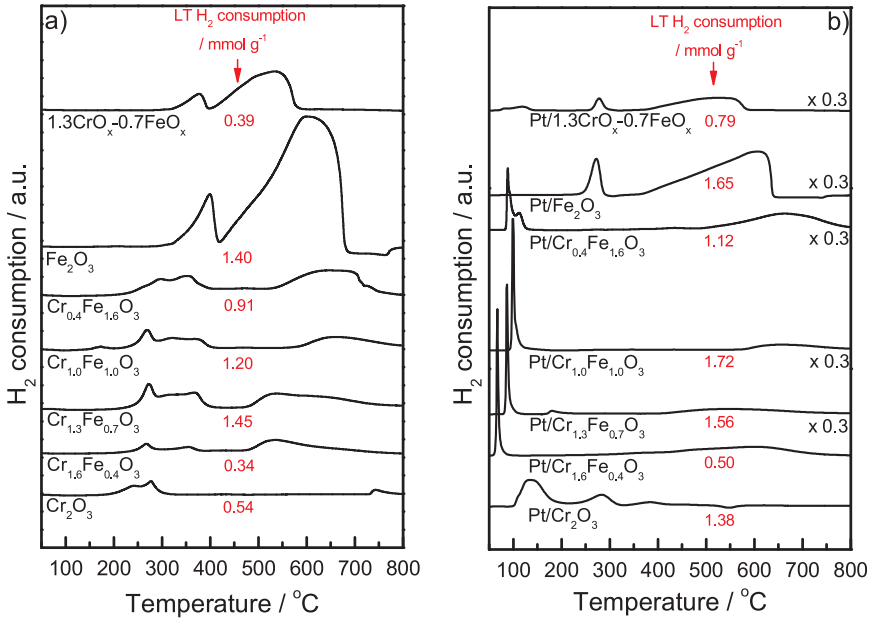

Fig. 3. H_2-TPR profiles of various supports and Pt catalysts.

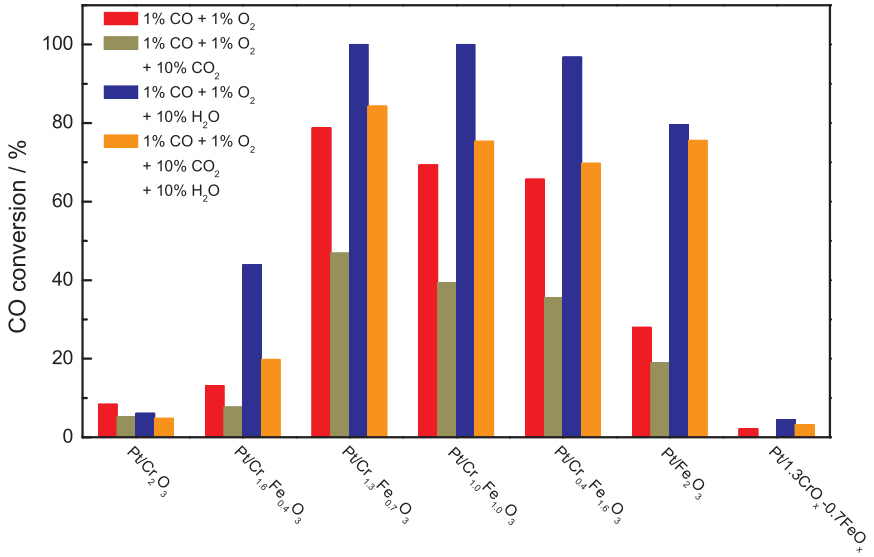

Fig. 4. Catalytic performance of various Pt catalysts under different reaction conditions. (T = 80 °C, data taken after 1 h reaction).

CO + 1% O_2 condition, the Pt/Cr_2O_3 catalyst shows very low CO conversion (8.5%); while the addition of Fe in the support significantly improves the activity, and the CO conversion reaches a maximum at the Pt/$Cr_{1.3}Fe_{0.7}O_3$ catalyst (78.8%); but the Pt/Fe_2O_3 catalyst is less active (28.0%). The specific reaction rate of the Pt/$Cr_{1.3}Fe_{0.7}O_3$ catalyst is 5.45×10^{-4} mol^{-1} g_{Pt}^{-1} s^{-1}, and the turnover frequency (TOF) is 0.203 s^{-1}. These values are higher than those reported in literature (i.e. 6.56×10^{-5} mol^{-1} g_{Pt}^{-1} s^{-1} and 0.023 s^{-1} on a Pt/TiO_2 catalyst [39]; 2.48×10^{-5} mol^{-1} g_{Pt}^{-1} s^{-1} and 0.0048 s^{-1} on a Pt/CeO_2 catalyst [40]; 6.69×10^{-5} mol^{-1} g_{Pt}^{-1} s^{-1} and 0.166 s^{-1} on a Pt/CoO_x/TiO_2 catalyst [41]; 2.01×10^{-4} mol^{-1} g_{Pt}^{-1} s^{-1} and 0.061 s^{-1} on a Pt/TiO_2-101 catalyst [42]; 8.65×10^{-5} mol^{-1} g_{Pt}^{-1} s^{-1} and 0.017 s^{-1} on a Pt/θ-Al_2O_3 catalyst [43]). The TOFs of other catalysts are also summarized in Table 1. It is also noted that the Pt/1.3CrO_x-0.7FeO_x is much less active than the Pt/$Ce_{1.3}Fe_{0.7}O_3$, which reflects the advantage of the $Cr_{1.3}Fe_{0.7}O_3$ support. 2. Under 1% CO + 1% O_2 + 10% CO_2 condition, drastic decline in activity are observed on all catalysts. 3. Under 1% CO + 1% O_2 + 10% H_2O condition, the activity could be greatly improved, except for the Pt/CrO_x catalyst. The possible water gas shift (WGS) reaction is ruled out because the reaction between CO and H_2O is negligible when the reaction temperature is below 120 °C (Fig. S4). 4. Under 1% CO + 1% O_2 + 10% CO_2 + 10% H_2O condition, the activity is lower than that in the presence of H_2O alone, but it is still higher than that under the 1% CO + 1% O_2 condition. The light-off curves of the Pt/$Cr_{1.3}Fe_{0.7}O_3$ catalyst under different reaction conditions are shown in Fig. S5, which further confirms the inhibiting role of CO_2 and the promoting role of H_2O at temperature range of 40–120 °C. The thermal stability of the Pt/$Cr_{1.3}Fe_{0.7}O_3$ catalyst is also investigated. As shown in Fig. S6, the activity of the catalyst calcined at 600 °C is less active than that calcined at 300 °C, probably due to the sintering of Pt particles and/or the structural change of the support under high temperature. Nevertheless, the aged catalyst is still tolerant to high concentrations of CO_2 and H_2O.

The different behaviors of the catalysts under CO + O_2 condition are worth of a discussion. CO oxidation over metal supported on reducible oxides has been extensively investigated in literature, and it is well recognized that the CO oxidation takes place via a metal-support interfacial route, in which the metal species provide centers for CO chemisorption while the support oxides provide centers for O_2 activation or the lattice oxygen of the support directly participate in the reaction [44–47]. However, the roles of the metal and supports in the reaction are rather complicated. For example, the interaction between the metal and support would change the morphology, particle size and the electronic properties of the metal, which could significantly affect the observed catalytic behaviors [48]. Moreover, the properties of the support such as surface area, crystal structure and exposed facet could also exert remarkable impacts on the catalytic behaviors. Supports with high surface areas are usually beneficial for the dispersion of metal species and thus small particle size. Also, it was reported that crystal structure of the support is important. Zhao et al. [49] compared the performance of Au, Pt and Rh supported on γ-Fe_2O_3 and α-Fe_2O_3, and they found that the catalysts on γ-Fe_2O_3 are more active than those on α-Fe_2O_3, due to their higher redox properties at low temperature. The catalysts employed in this work are very different due to various supports, and thus it is difficult to establish a precise structure-performance correlation. Nevertheless, a brief discussion on the roles of support in determining the properties of metal particles and catalyst reducibility could be made, since these parameters are very important in governing the activity [50]. First of all, it is found that the Pt particle sizes in the catalysts are similar (ca. 2 nm, Table 1, except for the Pt/Fe_2O_3 where the Pt particle size is about 2.6 nm) in spite of very different surface areas (17–52 m^2 g^{-1}), suggesting that the supports with different surface areas barely alter the Pt dispersion. However, the supports change the electronic properties of the Pt species, as the XPS results (Fig. S2) clear show that the fresh Pt/$Cr_{1.3}Fe_{0.7}O_3$ and Pt/Cr_2O_3 catalysts contain mostly Pt^{4+} species while the Pt/Fe_2O_3 contains a mixture of Pt^{2+} and Pt^{4+} species. Second, the catalyst reducibility is indeed significantly affected by the crystal phase and surface area of the support, which is clearly evidenced by the H_2-TPR results (Fig. 3). On one hand, the H_2 consumption of the catalyst roughly follows the surface area (the catalyst with higher surface area generally has higher H_2 consumption, Fig. 3b), probably due to more defects on the high-surface-area support because of its smaller crystallite size. On the other hand, the supports with different surface areas remarkably change the initial reduction temperatures of the catalysts, although no obvious relation could be established. Fig. 5 illustrates the correlation between LT - H_2 consumption, initial reduction temperature and TOFs of the catalysts. It seems that the activity of the catalyst is synergistically influenced by the two parameters. The catalysts (i.e. Pt/$Cr_{1.3}Fe_{0.7}O_3$, Pt/$Cr_{0.4}Fe_{1.6}O_3$ and Pt/$Cr_{1.0}Fe_{1.0}O_3$) with both low initial reduction temperatures (easy oxygen activation) and high H_2 consumptions (high amount of active oxygen) are more active. In contrast, other catalysts with high H_2 consumption but high initial reduction temperature (i.e. Pt/Fe_2O_3), or low initial reduction temperature but low H_2 consumption (i.e. Pt/Cr_2O_3 and Pt/$Cr_{1.6}Fe_{0.4}O_3$) are less active. Such correlation reflects the importance of the enhanced reducibility (low reduction temperature and high H_2 consumption) by the CrO_x-FeO_x interaction, which could

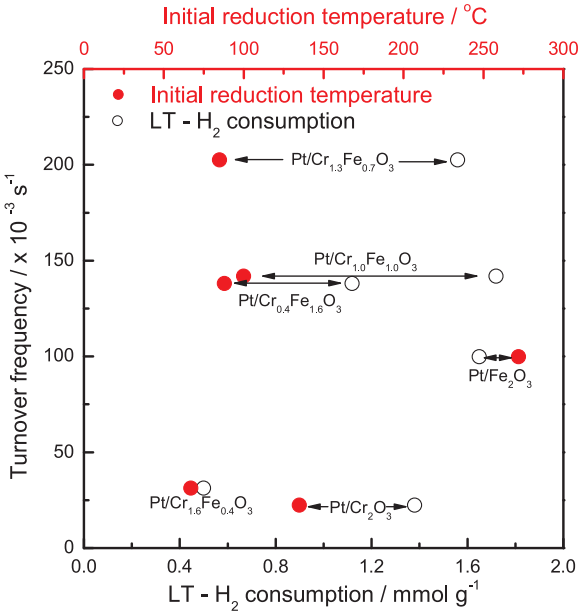

Fig. 5. Correlation between LT - H_2 consumption, initial reduction temperature and turnover frequency of various Pt catalysts at 80 °C.

explain the best performance observed on the $Pt/Cr_{1.3}Fe_{0.7}O_3$ catalyst. Moreover, this correlation highlights the roles of the support properties (such as crystal phase, surface area and crystallite size) in determining the catalytic behaviors.

The inhibiting role of CO_2 in the reaction was investigated, taken the $Pt/Cr_{1.3}Fe_{0.7}O_3$ catalyst as an example. As shown in Fig. 6a, the catalyst is stable for at least 10 h reaction under 1% CO + 1% O_2 + 10% CO_2 + 10% H_2O condition, while it gradually deactivates under 1% CO + 1% O_2 condition. The maintained stability in the presence of CO_2 and H_2O brings good potential for practical application in realistic conditions. The deactivation of the catalyst under 1% CO + 1% O_2 condition was further investigated via staged reaction. As shown in Fig. 6b, the $Pt/Cr_{1.3}Fe_{0.7}O_3$ catalyst is stable in the first 2 h reaction under CO + O_2 with the CO conversion of c.a. 72% (stage 1). When 10% of CO_2 is introduced in the feed stream, the activity rapidly decreases in the following 6 h with the CO conversion of c.a. 22% (stage 2), suggesting the deactivation of catalyst. Then, the CO_2 was removed from the feed stream and the reactants were restored to CO + O_2 (stage 3). The initial CO conversion increases to c.a. 30% but it starts declining after 1 h reaction. The observations in stage 1–3 reflects that the inhibiting role of CO_2 might be attributed to the following facts: 1, competitive adsorption of CO_2 with CO could take place, and thus occupy the active sites. However, the adsorption of CO_2 seems reversible because the activity could be partly recovered. Such competitive adsorption will be further discussed based on the kinetic results. 2, the formation of surface carbonate species during the reaction which would block the active sites [51,52]. After the reaction gases were stop and the catalyst was treated with 10% H_2O vapor at 80 °C for 1 h (stage 4), the catalytic activity could be fully recovered (stage 5). This indicates that the introduction of H_2O could effectively decompose the surface carbonate species and thus restore the activity [25].

To explain the effects of CO_2 and H_2O in the reaction, surface species of the $Pt/Cr_{1.3}Fe_{0.7}O_3$ catalyst in situ pretreated under different conditions were analyzed by XPS and the results are shown in Fig. 7. The C 1 s spectra (Fig. 7a) show two distinct components at BEs of 284.8 and 288.4 eV, which are assigned to adventitious carbon and carbonate [53]. Also, the surface composition of the carbonate increases from 27.4% in the pre-reduced sample to 39.8% after being treated with 10% CO_2 at 80 °C for 1 h, which indicates the formation of surface carbonates. When this sample was further treated with 10% water vapor at 80 °C for 1 h, the surface carbonate declines to 25.7%, suggesting that H_2O can effectively decompose the surface carbonate. As for the O 1 s spectra (Fig. 7b), all the spectra show one dominant component at BE of 529.9 eV and two weak components at BEs of 531.5 and 533.0 eV, which are assigned to lattice oxygen, surface hydroxyl groups and surface carbonates, respectively [54,55]. Also, the surface composition of carbonate oxygen increases from 7.6 to 11.8% after the CO_2 treatment while it significantly declines to 2.7% after the subsequent H_2O treatment, again confirming the decomposition of surface carbonate by H_2O addition. Moreover, the addition of H_2O remarkably increases the concentration of surface hydroxyl group, as the highest value (29.2%) was obtained (note that the increased hydroxyl concentration 23.9% after CO_2 treatment might be due to the low content of H_2O in the feed). Therefore, these XPS results clearly clarify the observed catalytic behaviors in Fig. 6. In addition, the formation of surface hydroxyl groups by H_2O addition is also evidenced, probably due to H_2O dissociation on the catalyst surface [56].

Figure S7 shows the Pt 4f spectra of the spent $Pt/Cr_{1.3}Fe_{0.7}O_3$ catalyst under different conditions. The spent catalyst under CO + O_2 and CO + O_2 + CO_2 conditions shows dominantly oxidized Pt species (Pt^{2+} and Pt^{4+}), while it shows the maintenance of metallic Pt° species under H_2O-containing conditions. These results indicate that the metallic Pt° after the pre-reduction (Table S1) could be re-oxidized in the presence

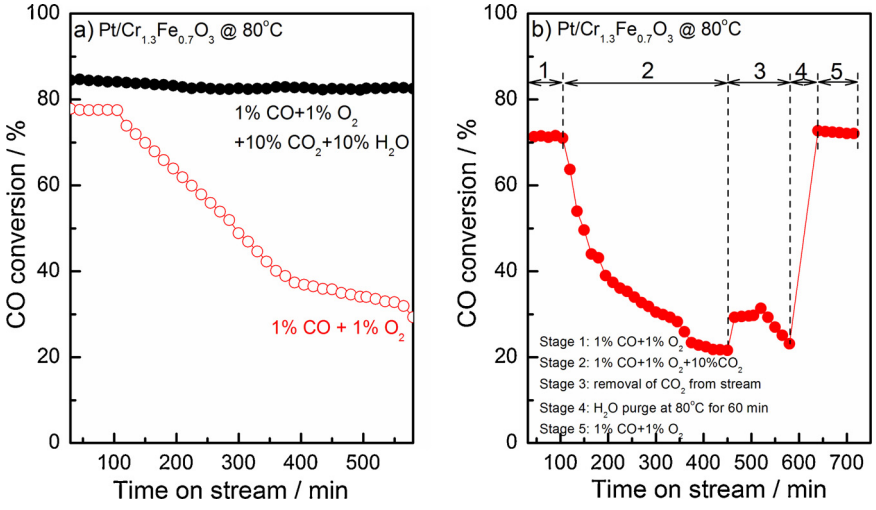

Fig. 6. a) Stability of $Pt/Cr_{1.3}Fe_{0.7}O_3$ catalyst under CO + O_2 and CO + O_2 + CO_2 + H_2O conditions; b) Catalytic behaviors of $Pt/Cr_{1.3}Fe_{0.7}O_3$ catalyst under different reaction conditions. S.V. = 120000 ml g^{-1} h^{-1}.

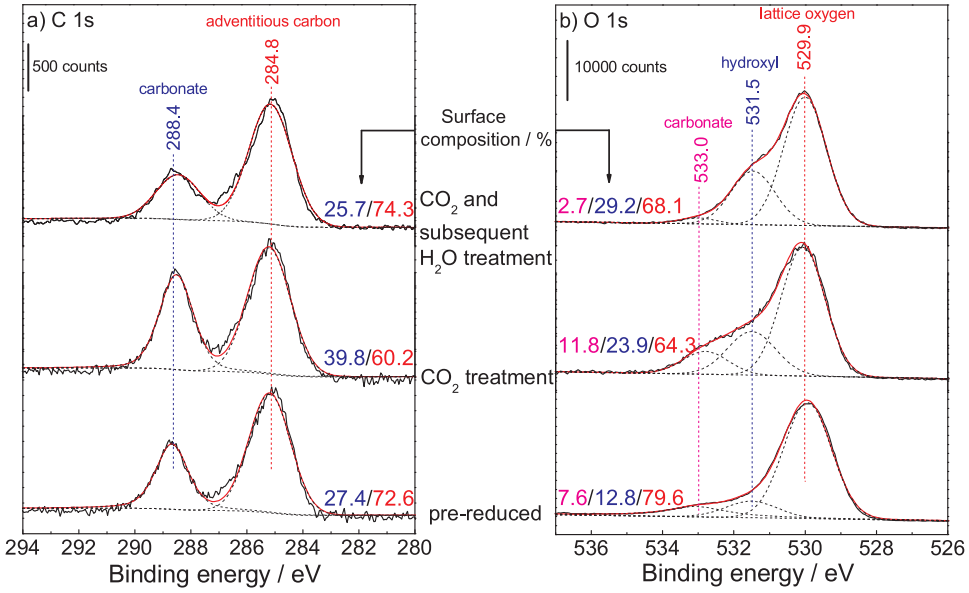

Fig. 7. a) C 1 s and b) O 1 s XPS spectra of $Pt/Cr_{1.3}Fe_{0.7}O_3$ catalyst in situ pretreated under different conditions.

of O_2. Somehow, the presence of H_2O in the feed could retain such metallic Pt species even in the presence of O_2. The presence of Pt° species under H_2O-containing environment might be one reason for the enhanced activity, as it was reported that the metallic Pt species are more active than the oxidized Pt species [57]

CO-TPD experiments were conducted on the $Pt/Cr_{1.3}Fe_{0.7}O_3$ catalyst to investigate the adsorption behaviors of the reactants on the catalyst. For the pre-reduced catalyst (Fig. 8a), the pre-adsorption of 1% CO results in distinct desorption of CO and CO_2 at about 75 °C, and the formation of CO_2 indicates the participation of lattice oxygen in the reaction. Additional O_2-TPD experiments (Fig. S8) shows that the pre-reduced $Pt/Cr_{1.3}Fe_{0.7}O_3$ catalyst gives a weak O_2 desorption signal at 330 °C, suggesting that the thermal depletion of oxygen is difficult. However, it should be noted that the depletion of lattice oxygen could be much easier when strong reducing agent (i.e. CO) is present, particularly at the metal-support interface. A similar scenario is that the active oxygen species in CO oxidation over a Au/TiO_2 catalyst are found to be the surface lattice oxygen at the Au-TiO_2 interface, which could easily react with CO at low temperature (i.e. 80 °C) [42]. The involvement of lattice oxygen in the reaction will be further discussed based on the kinetic results in the next section. The pre-adsorption of 1% CO + 10% H_2O results in desorption of CO and CO_2 emerges at 53 °C. However, the pre-adsorption of 1% CO + 10% CO_2 results in no desorption of CO in the temperature range of 50–300 °C, implying the presence of CO_2 in the feed dramatically suppresses the adsorption of CO on the surface. Compared to the case of pre-adsorption of 1% CO, the pre-adsorption of 1% CO + 10% H_2O results in several differences. 1. The lower CO desorption temperature (53 versus 75 °C) suggesting that the presence of H_2O in the feed somehow weakens the strength of CO-surface interaction and makes the CO easier to desorb. Indeed, the alleviation of CO self-poisoning on supported Pt catalyst by co-adsorption of H_2O was reported by Bergeld et al. [58]. 2. The peak areas of (CO + CO_2) is smaller under pre-adsorption of 1% CO + 10% H_2O than those under 1% CO pre-adsorption, indicating that H_2O suppressed

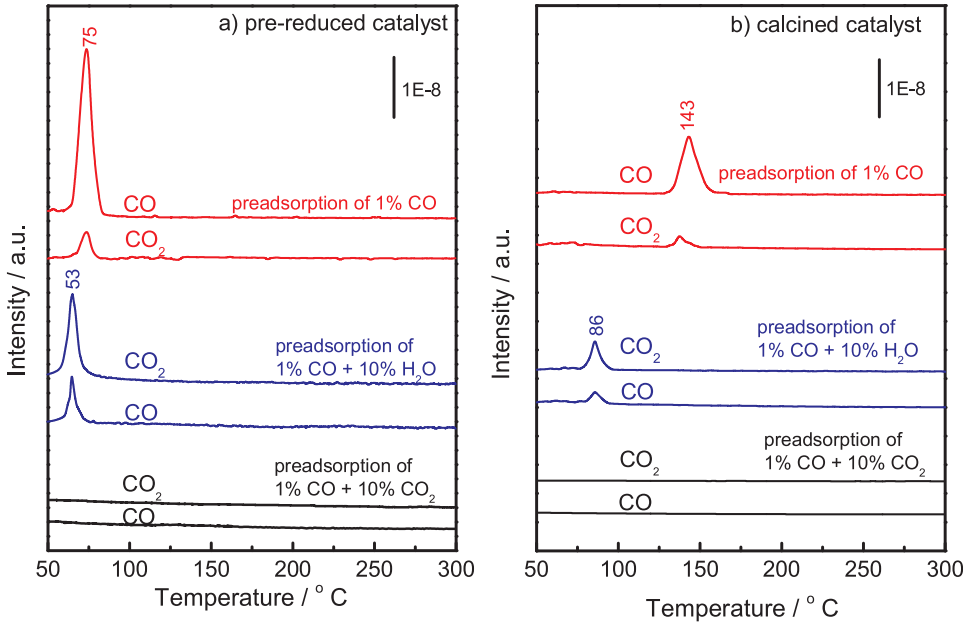

Fig. 8. CO-TPD profiles of a) pre-reduced and b) calcined $Pt/Cr_{1.3}Fe_{0.7}O_3$ catalyst under pre-adsorption of 1% CO, 1% CO + 10% H_2O and 1% CO + 10% CO_2.

the adsorption of CO. 3. The signal of CO_2 in case of 1% CO + 10% H_2O pre-adsorption is stronger than that in case of 1% CO pre-adsorption, suggesting that H_2O could effectively promotes the formation of CO_2. For the calcined catalyst (Fig. 8b), the preadsorption of 1% CO results in simultaneous desorptions of CO and CO_2 at 143 °C, while the pre-adsorption of 1% CO + 10% H_2O results in desorption of CO and CO_2 at 86 °C. Again, the lowered desorption temperature on the latter case suggests the weakened CO adsorption strength (easier desorption of CO) and promoted CO oxidation activity (lower temperature for CO_2 formation) in the presence of H_2O, but the lower signal intensity implies the suppression of CO adsorption in the presence of H_2O which is similarly observed on the pre-reduced catalyst. Moreover, the comparison of Fig. 8a and b clearly reflects the following facts. 1. The adsorption amount on the calcined catalyst is much lower than that on the pre-reduced one, due to the lack of metallic Pt species in the calcined catalyst which easily adsorb CO molecules (Fig. S2) [57]. 2. The higher desorption temperature of CO_2 on the calcined catalyst indicates that calcined catalyst is less active than the pre-reduced one, due to the presence of Pt oxide in the calcined catalyst [57]. Indeed, the light-off curves of the pre-reduced and calcined 2 $Pt/Cr_{1.3}Fe_{0.7}O_3$ catalyst (Fig. S9) show that the pre-reduced catalyst is more active than the calcined one under any reaction conditions.

3.3. Kinetic study

Reaction kinetics were employed on the representative $Pt/Cr_{1.3}Fe_{0.7}O_3$ catalyst to further clarify its intrinsic catalytic behaviors and the roles of CO_2 and H_2O in the reaction. First, the role of CO_2 was investigated. Based on the results in Table S2, the power law rate expression is $r = 1.61 \times 10^{-6}\ [CO]^{0.79}[O_2]^{0.06}[CO_2]^{-0.23}$, and the negative reaction order of CO_2 suggests CO_2 could inhibit the activity. In contrast, the presence of H_2O (without CO_2 in the feed, Table S3) leads to a power law rate expression of $r = 3.21 \times 10^{-6}\ [CO]^{0.72}[O_2]^{0.08}[H_2O]^{0.25}$, and the positive reaction order of H_2O clearly suggests its promoting role in the reaction. We also investigated the effect of H_2O on the reaction order of CO_2. Based on the kinetic data in Table S4, under the reaction condition of 1% CO + 1% O_2 + 10% H_2O, the reaction rate declines with increasing CO_2 content in the feed stream. However, the reaction order of CO_2 is -0.11 ± 0.01 (Fig. S10), which is slightly higher than that under dry condition (-0.23). This means the addition of H_2O in the feed stream suppresses the adsorption of CO_2 on the catalyst surface and thus alleviates the inhibiting role of CO_2, which are consistent with the observed catalytic behaviors (Fig. 4).

Table 2 summarizes the apparent reaction constant (k_{app}) and reaction orders of CO and O_2 of the $Pt/Cr_{1.3}Fe_{0.7}O_3$ catalyst under different reaction conditions at 60 °C (See Table S5 and Fig. S11 for details). Compared to the CO + O_2 condition, the k_{app} declines to 1.61×10^{-6} in the presence of 10% CO_2; while the values become higher in the presence of 10% H_2O (3.08–3.21 $\times 10^{-6}$, with or without the presence of 10% CO_2). Concerning the reaction orders, the presence of CO_2 and/or H_2O in the feed results in higher reaction order of CO (0.72 - 0.79 versus 0.39), while it hardly changes that of O_2 (near zero).

Table 2
Kinetic results of $Pt/Cr_{1.3}Fe_{0.7}O_3$ catalyst under different reaction conditions.

$Pt/Cr_{1.3}Fe_{0.7}O_3$ T = 60 °C $r = k_{app}\ [CO]^a\ [O_2]^b$

Reaction conditions	k_{app} / x 10^{-6}	a	b	Ea / kJ mol^{-1}
CO + O_2	2.68	0.39 ± 0.05	0.04 ± 0.01	26.4 ± 1.5
CO + O_2 + 10 % CO_2	1.61	0.79 ± 0.06	0.06 ± 0.01	27.8 ± 2.1
CO + O_2 + 10 % H_2O	3.21	0.72 ± 0.08	0.04 ± 0.02	15.5 ± 1.1
CO + O_2 + 10 % CO_2 + 10 % H_2O	3.08	0.78 ± 0.09	0.05 ± 0.01	19.4 ± 1.4

The validity of the parameters are confirmed by the parity plots and residual analyses (Table S6) and the calculated Eas (Table 2) reveal that the Ea is 26.4 ± 1.5 kJ mol^{-1} under CO + O_2, which is slightly lower than that in the presence of 10% CO_2 in the feed (27.8 ± 2.1 kJ mol^{-1}) but much higher than those in the presence of 10% H_2O in the feed (15.5 ± 1.1 kJ mol^{-1} for the addition of 10% H_2O, and 19.4 ± 1.4 kJ mol^{-1} for the addition of 10% H_2O + 10% CO_2), which further confirms the inhibiting effect of CO_2 and the promoting effect of H_2O.

Based on the above results, the elementary steps of CO oxidation under various conditions could be deduced. The mechanisms of CO oxidation over supported Pt catalysts have been extensively investigated in literature, which could be categorized into two groups. When Pt is supported on inert oxides such as SiO_2 and Al_2O_3, the reaction pathways usually involve competitive or non-competitive adsorption of CO and O_2 on the surface Pt atoms [59–61]. In contrast, when Pt is supported on reducible oxides such as CeO_2, Fe_2O_3 and TiO_2, the reaction is believed to take place at metal-support interface (so-called "interfacial reaction"), which usually involves a reaction of CO chemisorbed on surface Pt atoms and the oxygen species chemisorbed on the support [39] or lattice oxygen provided by the support [42]. In the latter case (participation of lattice oxygen), the reaction order of oxygen is zero and thus a Mars van-Krevelen mechanism (M—K mechanism) is proposed [42]. The current results show that the reaction orders of O_2 under various conditions remain zero, which implies that the CO oxidation over the $Pt/Cr_{1.3}Fe_{0.7}O_3$ catalyst may follow a M-K mechanism. Therefore, elementary steps under CO + O_2 or CO + O_2 + CO_2 condition are proposed and summarized in Table 3.

For the reaction under CO + O_2 condition, the steps mainly include CO chemisorption on the surface Pt atom (eq. 1); the reaction between chemisorbed CO and lattice oxygen to form CO_2 (eq. 2); desorption of CO_2 from Pt surface (eq. 3); replenishment of oxygen vacancy by gaseous O_2 (eq. 4). Eq. 2 is considered as the rate determining step (RDS) and thus the rate expression is

$$r = kK_{CO}P_{CO}\ [M\text{-}O]/(1 + K_{CO}P_{CO} + K_{CO2}P_{CO2}),$$

where [M-O] is the concentration of lattice oxygen on the catalyst surface (calculated to be 0.37, based on the XPS results in Table S1), K_{CO} and K_{CO2} are the adsorption equilibrium constants of CO and CO_2,

Table 3
Proposed elementary steps on $Pt/Cr_{1.3}Fe_{0.7}O_3$ catalyst under different conditions.

Under CO + O_2 or CO + O_2 + CO_2	
$2[CO + Pt^* \overset{K_{CO}}{\longleftrightarrow} CO - Pt]$	(eq. 1)
$2[CO - Pt + M - [O] \overset{k}{\longrightarrow} CO_2 - Pt + M - []]$	(eq. 2) RDS
$2[CO_2 - Pt \overset{K_{CO2}^{-1}}{\longleftrightarrow} CO_2 + Pt^*]$	(eq. 3)
$O_2 + 2M - [] \rightarrow 2M - [O]$	(eq. 4)
$2CO + O_2 \rightarrow 2CO_2$	Overall reaction
$r = kK_{CO}P_{CO}[M - O]/(1 + K_{CO}P_{CO} + K_{CO2}P_{CO2})$	Rate expression
Pt* refers to active site on Pt, M-[O] refers to lattice oxygen on the support	

Under CO + O_2 + H_2O [a]	
$2[CO + Pt^* \overset{K_{CO}}{\longleftrightarrow} CO - Pt]$	(eq. 1')
$2[H_2O + M - [O] \overset{K_{H2O}}{\longleftrightarrow} HO - M - [O] - H]$	(eq. 2')
$2[CO - Pt + HO - M - [O] - H \overset{k}{\longrightarrow} COOH - Pt + M - [O] - H]$	(eq. 3') RDS
$2[COOH - Pt \rightarrow CO_2 + Pt - H]$	(eq. 4')
$2[Pt - H + M - [O] - H \rightarrow Pt^* + M - [] + H_2O]$	(eq. 5')
$2M - [] + O_2 \rightarrow 2M - [O]$	(eq. 6')
$2CO + O_2 \rightarrow 2CO_2$	Overall reaction
$r' = kK_{CO}P_{CO}K_{H2O}P_{H2O}/[(1 + K_{CO}P_{CO}) \times (1 + K_{H2O}P_{H2O})]$	Rate expression
Pt* refers to active site on Pt, M-[O] refers to lattice oxygen on the support	

[a]: The eqs. 1' - 6' only represent those H_2O-assisted steps.

Table 4
Derived kinetic parameters of $Pt/Cr_{1.3}Fe_{0.7}O_3$ catalyst under different reaction conditions (T = 60 °C).

Reaction conditions	k x 10^{-5} / mol g^{-1} s^{-1}	K_{CO} / kPa^{-1}	K_{CO2} / kPa^{-1}	K_{H2O} / kPa^{-1}
$CO + O_2$	1.43	1.25	–	–
$CO + O_2 + CO_2$	0.89	0.12	11.1	–
$CO + O_2 + H_2O$	4.50	0.15	–	11.1

respectively. The reaction rate increases with increasing partial pressure of CO but decreases with increasing partial pressure of CO_2, which is consistent with the observed kinetics. Furthermore, the kinetic parameters were derived using a non-linear regression method using the data in Table S2. As shown in Table 4, under $CO + O_2$ condition, note that the CO_2 concentration in the reaction is very low because of the low CO conversion, and thus the $r = kK_{CO}P_{CO}$ [M-O]/$(1 + K_{CO}P_{CO} + K_{CO2}P_{CO2})$ could be simplified to $r = kK_{CO}P_{CO}$ [M-O]/$(1 + K_{CO}P_{CO})$. The calculated rate constant k is 1.43×10^{-5} mol g^{-1} s^{-1}, and the adsorption equilibrium constant of CO (K_{CO}) is 1.25 kPa^{-1}. Under the condition of $CO + O_2 + CO_2$, the rate constant k declines to 0.89×10^{-5} mol g^{-1} s^{-1}, and the K_{CO} declines to 0.12 kPa^{-1}; meanwhile, the adsorption equilibrium constant of CO_2 (K_{CO2}) is 11.1 kPa^{-1}. Such phenomenon could be explained by the competitive adsorption of CO_2 with CO on the Pt surface, which leads to declined coverage of CO and thus declined activity.

It is interesting that the addition of H_2O improves the activity although it causes a lowered CO coverage as the CO reaction order increases from 0.39 to 0.72. Such competitive adsorption between CO and H_2O is confirmed by the CO-TPD results (Fig. 8b), suggesting that H_2O could adsorb on the surface Pt atoms. Since the WGS reaction is ruled out at low reaction temperature (Fig. S4) and the Ea value (15.5 kJ mol^{-1}, Table 2) in the presence of H_2O is much lower than that in the absence of H_2O (26.4 kJ mol^{-1}, Table 2), it could be expected that H_2O may participate in the reaction and thus open a pathway. In fact, the promoting effect of H_2O in CO oxidation has been reported [62–65]. For example, theoretical findings reported by Wang et al. [66] and Gong et al. [67] suggest a reaction between CO molecule and the hydroxyl group (-OH) formed by dissociation of H_2O on Pt(111) is much easier compared to that between CO and surface O species. However, in the current work, the reaction between CO and -OH group (both on surface Pt sites) could be ruled out because otherwise similar promoting effect of H_2O could also have been observed on the Pt/Cr_2O_3 catalyst. Alternatively, interfacial reaction between CO (on Pt atoms) and -OH groups (dissociated on oxide support) has been proposed to explain the promoting effect of H_2O, which has been experimentally confirmed by Jin et al. [23] and Lin et al [68], on a model FeO(111)/Pt(111) catalyst and a practical $Ir/Fe(OH)_x$ catalyst, respectively. In a very recent work by Wang et al. [24], CO oxidation was conducted over a single Pt atom Pt_1/CeO_2 catalyst and the promoting role of H_2O was attributed to the facile interfacial reaction between CO (on single Pt atom) and the -OH group (on CeO_2 support) from dissociated H_2O with a carboxyl intermediate, which followed a reaction pathway so called “water-mediated Mars - van Krevelen mechanism” [24]. In contrast, the H_2O-driven formation of hydroperoxyl species (-OOH) have been reported recently [26,69]. Ojeda et al. [26] concluded that H_2O acts as a co-catalyst essential for O_2 activation and for catalyst stability in CO oxidation over Au and Pt catalysts, and the formation of hydroperoxy intermediates (-OOH) is responsible for the improvement of activity. The authors also derived a rate expression of $r = \alpha(P_{CO}P_{O2}P_{H2O})^{2/3}/[1 + K_1P_{CO} + K_2P_{O2} + K_3P_{H2O}]^2$, in which the reaction rate depends on the concentrations of CO, O_2 and H_2O, and the increase of O_2 partial pressure would enhance the rate [26]. However, such kinetic model is in conflict with the kinetics observed in the current work, as the reaction rate is independent on the partial pressure of O_2 (Table 2).

Based on the literature survey and the obtained kinetics, we believe that the relevant H_2O-related kinetics mainly involve the dissociation of H_2O and the formation of -OH species on the support. In the current work, the possible formation of surface hydroxyl group induced by H_2O is confirmed by the XPS results (Fig.7b). Accordingly, the elementary steps under $CO + O_2 + H_2O$ are proposed in Table 3. The reaction sequences include the chemisorption of CO (eq. 1’); the formation of -OH species on the support via H_2O dissociation (eq. 2’); interfacial reaction between CO and -OH to form carboxyl species (-COOH) (RDS, eq. 3’); decomposition of -COOH to CO_2 and -H (eq. 4’); reaction between -H and -OH to form H_2O (eq. 5’) and replenishment of oxygen vacancy by gaseous O_2 (eq. 6’). If the CO chemisorption (eq. 1’) or the formation of -OH groups (eq. 2’) is the RDS, then the reaction rate would be respectively proportional to the partial pressure of CO or H_2O, which is not consistent with the observed kinetics. On the other hand, a recent DFT calculation [24] on H_2O-assisted CO oxidation over $Pt1/CeO_2$ catalyst reveals that the reaction between CO and -OH group needs a energy barrier of 0.48 eV and this step is the RDS, while the dehydrogenation of the carboxyl species (eq. 4’) is very fast (with a barrier of 0.16 eV). Therefore, the proposed elementary steps in the current work are reasonable. The resulting rate expression is $r = kK_{CO}P_{CO}K_{H2O}P_{H2O}/[(1 + K_{CO}P_{CO})(1 + K_{H2O}P_{H2O})]$

where K_{CO}, K_{H2O} are the adsorption equilibrium constants of CO and H_2O, respectively. The expression predicts that the reaction rate would increase with increasing partial pressures of CO and H_2O, which is consistent with the kinetic results (Table S3). The calculated kinetic parameters in Table 4 reveal that compared to those under $CO + O_2$ condition, the intrinsic rate constant k is increased by 3-fold (4.50×10^{-5} versus 1.43×10^{-5} mol g^{-1} s^{-1}), which well explains the enhanced activity by the H_2O addition. The CO adsorption equilibrium constant K_{CO} is decreased by 8-fold (0.15 versus 1.25 kPa^{-1}) while the adsorption equilibrium constant of H_2O (K_{H2O}) is high (11.1 kPa^{-1}), which validates the competitive adsorption of H_2O and CO on the surface Pt atoms.

Therefore, the roles of CO_2 and H_2O in the CO oxidation over the $Pt/Cr_{1.3}Fe_{0.7}O_3$ catalyst could be explicated. The deactivating effect of CO_2 is due to its competitive adsorption with CO and the formation of surface carbonates that block the active interfacial sites. On the contrary, the presence of H_2O in the feed stream sustains the catalyst stability, owing to its capability to decompose the carbonates. Besides, the promoting effect of H_2O in reactivity could be attributed to the following facts: 1, the addition of H_2O remains metallic Pt° species in the catalyst; 2, co-adsorption of H_2O with CO on surface Pt atoms weakens the strength of CO chemisorption although it lowers the CO coverage on the Pt surface atoms; 3, the interfacial reaction between CO and -OH groups via H_2O dissociation on the support surface. The reaction mechanisms under different conditions are illustrated in Fig. 9.

4. Conclusions

The $Pt/Cr_xFe_{2-x}O_3$ catalysts are active for CO oxidation, and their behaviors are closely related to the reducibility of the catalysts. More importantly, these catalysts are tolerant to high concentrations of CO_2 and H_2O, which may meet the requirement of practical applications. Various experiments were conducted in order to clarify the roles of CO_2 and H_2O in the reaction, and the main conclusions are as follows:

1 The addition of CO_2 in the feed leads to severe decline of activity and catalyst stability, owing to the competitive adsorption of CO_2 with CO and formation of carbonate species on catalyst surface.
2 The H_2O in the feed could effectively decompose the surface carbonate and thus maintain the catalyst stability.
3 H_2O molecules could adsorb on both surface Pt atoms and support surface, which could effectively improve the activity. The promoting role of H_2O is due to the maintainance of metallic Pt° species in the

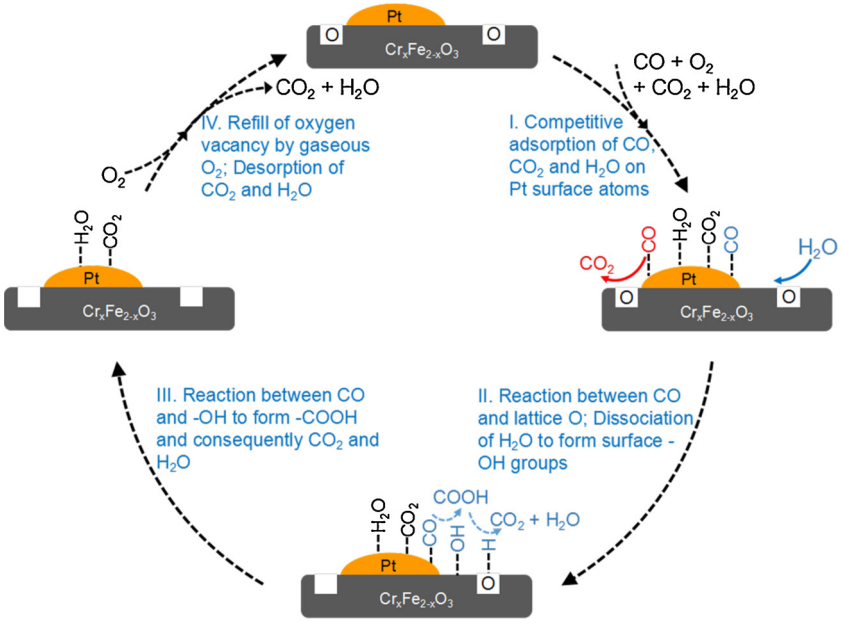

Fig. 9. Reaction pathways of CO oxidation over $Pt/Cr_{1.3}Fe_{0.7}O_3$ catalyst under different conditions.

catalyst, the weakened CO adsorption strength by the competitive adsorption of H_2O on the surface Pt atoms, and the fast interfacial reaction between CO and -OH groups formed via H_2O dissociation on the support surface.

Acknowledgement

This work is financially supported by the National Natural Science Foundation of China (No. 21643007 and 21773212).

Appendix A. Supplementary data

Supplementary material related to this article can be found, in the online version, at doi:https://doi.org/10.1016/j.apcatb.2018.12.054.

References

[1] M. Haruta, S. Tsubota, T. Kobayashi, H. Kageyama, M.J. Genet, B. Delmon, J. Catal. 144 (1993) 175–192.
[2] Y.H. Chen, C.Y. Mou, B.Z. Wan, Appl. Catal. B Environ. 218 (2017) 506–514.
[3] K. Yang, Y. Zhang, Y. Li, P. Huang, X. Chen, W. Dai, X. Fu, Appl. Catal. B Environ. 183 (2016) 206–215.
[4] L. Soler, A. Casanovas, A. Urrich, I. Angurell, J. Llorca, Appl. Catal. B Environ. 197 (2016) 47–55.
[5] E. del Río, A.B. Hungría, M. Tinoco, R. Manzorro, M.A. Cauqui, J.J. Calvino, J.A. Pérez-Omil, Appl. Catal. B Environ. 197 (2016) 86–94.
[6] F. Morfin, T.S. Nguyen, J.L. Rousset, L. Piccolo, Appl. Catal. B Environ. 197 (2016) 2–13.
[7] S.K. Meher, M. Cargnello, H. Troiani, T. Montini, G.R. Rao, P. Fornasiero, Appl. Catal. B Environ. 130-131 (2013) 121–131.
[8] E.O. Jardim, M. Gonçalves, S. Rico-Francés, A. Sepúlveda-Escribano, J. Silvestre-Albero, Appl. Catal. B Environ. 113-114 (2012) 72–78.
[9] Z. Ding, H. Yang, J. Liu, W. Dai, X. Chen, X. Wang, X. Fu, Appl. Catal. B Environ. 101 (2011) 326–332.
[10] C.H. Jung, J. Yun, K. Qadir, B. Naik, J.Y. Yun, J.Y. Park, Appl. Catal. B Environ. 154-155 (2014) 171–176.
[11] M.S. Chen, D.W. Goodman, Science 306 (2004) 252–255.
[12] D.R. Schryer, B.T. Upchurch, B.D. Sidney, K.G. Brown, G.B. Hoflund, R.K. Herz, J. Catal. 130 (1991) 314–317.
[13] K. Liu, A.Q. Wang, T. Zhang, ACS Catal. 2 (2012) 1165–1178.
[14] A. Di Benedetto, G. Landi, L. Lisi, G. Russo, Appl. Catal. B Environ. 142-143 (2013) 169–177.
[15] J.L. Ayastuy, A. Gil-Rodríguez, M.P. González-Marcos, M.A. Gutiérrez-Ortiz, Int. J. Hydro. Energy 31 (2006) 2231–2242.
[16] E.O. Jardim, S. Rico-Francés, F. Coloma, J.A. Anderson, E.V. Ramos-Fernandez, J. Silvestre-Albero, A. Sepúlveda-Escribano, Appl. Catal. A Gen. 492 (2015) 201–211.
[17] B. Qiao, A. Wang, L. Li, Q. Lin, H. Wei, J. Liu, T. Zhang, ACS Catal. 4 (2014) 2113–2117.
[18] A. Luengnaruemitchai, K. Srihamat, C. Pojanavaraphan, R. Wanchanthuek, Int. J. Hydro. Energy 40 (2015) 13443–13455.
[19] F. Boccuzzi, A. Chiorino, M. Manzoli, P. Lu, T. Akita, S. Ichikawa, M. Haruta, J. Cat al. 202 (2001) 256–267.
[20] P. Landon, J. Fergusson, B.E. Solsona, T. Garcia, S. Al-Sayari, A.F. Carley, A.A. Herzing, C.J. Kiely, M. Makkee, J.A. Moulijn, A. Overweg, S.E. Golunski, G.J. Hutchings, J. Mater. Chem. 16 (2006) 199–208.
[21] M. Daté, M. Haruta, J. Catal. 201 (2001) 221–224.
[22] M. Daté, M. Okumura, S. Tsubota, M. Haruta, Angew. Chem. Int. Ed. 43 (2004) 2129–2132.
[23] Y. Jin, G. Sun, F. Xiong, L. Ding, W. Huang, J. Phys. Chem. C 120 (2016) 9845–9851.
[24] C. Wang, X.K. Gu, H. Yan, Y. Lin, J. Li, D. Liu, W.X. Li, J. Lu, ACS Catal. 7 (2017) 887–891.
[25] T. Fujitani, I. Nakamura, M. Haruta, Catal. Lett. 144 (2014) 1475–1486.
[26] M. Ojeda, B.Z. Zhan, E. Iglesia, J. Catal. 285 (2012) 92–102.
[27] L. Liu, F. Zhou, L. Wang, X. Qi, F. Shi, Y. Deng, J. Cata l. 274 (2010) 1–10.
[28] K. Liu, A. Wang, W. Zhang, J. Wang, Y. Huang, X. Wang, J. Shen, T. Zhang, Ind. Eng. Chem. Res. 50 (2011) 758–766.
[29] C. Qi, S. Zhu, H. Su, H. Lin, R. Guan, Appl. Catal. B Environ. 138-139 (2013) 104–112.
[30] G. Xanthopoulou, G. Vekinis, Appl. Catal. B Environ. 19 (1998) 37–44.
[31] G. Pantaleo, L.F. Liotta, A.M. Venezia, G. Deganello, E.M. Ezzo, M.A. El Kherbawi, H. Atia, Mater. Chem. Phys. 114 (2009) 604–611.
[32] Y. Wang, A.P. Jia, M.F. Luo, J.Q. Lu, Appl. Catal. B Environ. 165 (2015) 477–486.
[33] Y. Wu, X. Wang, Mater. Lett. 65 (2011) 2062–2065.
[34] J. Chen, X. Zhang, H. Arandiyan, Y. Peng, H. Chang, J. Li, Catal. Today (2013) 201 12-20118.
[35] P. Li, D.E. Miser, S. Rabiei, R.T. Yadav, M.R. Hajaligol, Appl. Catal. B Environ. 43 (2003) 151–162.
[36] J. Zieliński, I. Zglinicka, L. Znaka, Z. Kaszkur, Appl. Catal. A Gen. 381 (2010) 191–196.
[37] L. Liu, F. Zhou, L. Wang, X. Qi, F. Shi, Y. Deng, J. Catal. 274 (2010) 1–10.
[38] D. Jain, G. Madras, Ind. Eng. Chem. Res. 56 (2017) 2008–2024.
[39] N. Li, Q.Y. Chen, L.F. Luo, W.X. Huang, M.F. Luo, G.S. Hu, J.Q. Lu, Appl. Catal. B Environ. 142-143 (2013) 523–532.
[40] L. Nie, D. Mei, H. Xiong, B. Peng, Z. Ren, X.I.P. Hernandez, A. DeLaRiva, M. Wang, M.H. Engelhard, L. Kovarik, A.K. Datye, Y. Wang, Science 358 (2017) 1419–1423.
[41] H. Qin, X. Qian, T. Meng, Y. Lin, Z. Ma, Catalysts 5 (2015) 606–633.
[42] Y. Zhou, D.E. Doronkin, M. Chen, S. Wei, J.D. Grunwaldt, ACS Catal. 6 (2016) 7799–7809.
[43] M. Moses-DeBusk, M. Yoon, L.F. Allard, D.R. Mullins, Z. Wu, X. Yang, G. Veith, G.M. Stocks, C.K. Narula, J. Am. Chem. Soc. 135 (2013) 12634–12645.
[44] M. Kotobuki, R. Leppelt, D.A. Hansgen, D. Widmann, R.J. Behm, J. Catal. 264 (2009) 67–76.
[45] D. Widmann, R.J. Behm, Angew. Chem. Int. Ed. 50 (2011) 10241–10245.
[46] H.H. Liu, Y. Wang, A.P. Jia, S.Y. Wang, M.F. Luo, J.Q. Lu, Appl. Surf. Sci. 314 (2014) 725–734.
[47] Y. Maeda, Y. Iizuka, M. Kohyama, J. Am. Chem. Soc. 135 (2013) 906–909.
[48] J. Kugai, T. Moriya, S. Seino, T. Nakagawa, Y. Ohkubo, H. Nitani, Y. Mizukoshi, T.A. Yamamoto, Appl. Catal. B Environ. 126 (2012) 306–314.
[49] K. Zhao, H. Tang, B. Qiao, L. Li, J. Wang, ACS Catal. 5 (2015) 3528–3539.

[50] M. Haruta, N. Yamada, T. Kobayashi, S. Iijima, J. Catal. 115 (1989) 301–309.
[51] F. Boccuzzi, A. Chiorino, M. Manzoli, P. Lu, T. Akita, S. Ichikawa, M. Haruta, J. Catal. 202 (2001) 256–267.
[52] D. Gamarra, A. Martínez-Arias, J. Catal. 263 (2009) 189–195.
[53] K. Mudiyanselage, S.D. Senanayake, L. Feria, S. Kundu, E. Baber, J. Graciani, A.B. Vidal, S. Agnoli, J. Evans, R. Chang, S. Axnanda, Z. Liu, J.F. Sanz, P. Liu, J.A. Rodriguez, D.J. Stacchiola, Angew. Chem. Int. Ed. 52 (2013) 5101–5105.
[54] L. Qi, B. Cheng, J. Yu, W. Ho, J. Hazard. Mater. 301 (2016) 522–530.
[55] C.A. Chagas, E.F. Souza, R.L. Manfro, S.M. Landi, M.M. Souza, M. Schmal, Appl. Catal. B Environ. 182 (2016) 257–265.
[56] S.C. Ammal, A. Heyden, ACS Catal. 4 (2014) 3654–3662.
[57] G.J. Kim, D.W. Kwon, S.C. Hong, J. Phys. Chem. C 120 (2016) 17996–18004.
[58] J. Bergeld, B. Kasemo, D.V. Chakarov, Surf. Sci. 495 (2001) L815–L820.
[59] A.D. Allian, K. Takanabe, K.L. Fujdala, X. Hao, T.J. Truex, J. Cai, C. Buda, M. Neurock, E. Iglesia, J. Am. Chem. Soc. 133 (2011) 4498–4517.
[60] F.J. Gracia, J.T. Miller, A.J. Krof, E.E. Wolf, J. Catal. 209 (2002) 341–354.
[61] G. Djega-Mariadassou, M. Boudart, J. Catal. 216 (2003) 89–97.
[62] J. Saavedra, H.A. Doan, C.J. Pursell, L.C. Grabow, B.D. Chandler, Science 345 (2014) 1599–1602.
[63] H.Y. Su, M.M. Yang, X.H. Bao, W.X. Li, J. Phys. Chem. C 112 (2008) 17303–17310.
[64] L.M. Liu, B. McAllister, H.Q. Ye, P. Hu, J. Am. Chem. Soc. 128 (2006) 4017–4022.
[65] C. Shang, Z.P. Liu, J. Phys. Chem. C 114 (2010) 16989–16995.
[66] H.F. Wang, R. Kavanagh, Y.L. Guo, Y. Guo, G.Z. Lu, P. Hu, Angew. Chem. Int. Ed. 51 (2012) 6657–6661.
[67] X.Q. Gong, P. Hu, R. Raval, J. Chem. Phys. 119 (2002) 6324–6334.
[68] J. Lin, B. Qiao, L. Li, H. Guan, C. Ruan, A. Wang, W. Zhang, X. Wang, T. Zhang, J. Catal. 319 (2014) 142–149.
[69] T.M. Tran-Thuy, C.C. Chen, S.D. Lin, ACS Catal. 7 (2017) 4304–4312.